Summer 2013

Fabry-Perot Interferometer based CO_2 Sensor using Ionic-liquid

Mujahid Abdul

Department:

FABRY-PEROT INTERFEROMETER BASED CO_2 SENSOR USING IONIC LIQUID

by

MUJAHID ABDUL

A THESIS

Presented to the Graduate Faculty of the

MISSOURI UNIVERSITY OF SCIENCE AND TECHNOLOGY

In Partial Fulfillment of the Requirements for the Degree

MASTER OF SCIENCE IN ELECTRICAL ENGINEERING

2013

Approved by

Dr. Hai Xiao, Advisor
Dr. Mehdi. Ferdowsi
Dr. Maciej J. Zawodniok

ABSTRACT

Anthropogenic greenhouse gas emission has become an eminent problem today especially CO_2 gas emission is of major importance. Statistics show that CO_2 concentration is consistently increasing in atmosphere every year. Having cognizance of this problem, better CO_2 absorbents, ionic liquids, has been suggested through this thesis. To prove Ionic liquid's efficiency, a unique sensor was developed by a sophisticated fabrication using Femto-second (fs) laser. Sensor is built to work as an extrinsic Fabry-Perot Interferometer (EFPI) to sense CO_2.

EFPI sensor consists of a glass tube fused between two single mode fibers, and a miniature hole is fabricated in the tube using fs-laser to admit ionic liquids as medium. EFPI works on the principle of the changes encountered by the light reflected back from the flat surfaces of the fiber at the two walls of the tube thus resulting in a wavelength shift in the original spectrum. This interference will strongly be affected by change in any optical property of the medium.

As a medium of EFPI, Ionic liquid is exposed to CO_2 through the fabricated hole and resultant shift in wavelength of the spectrum is referred to as a change in refractive index of Ionic liquid due to CO_2 absorption. Dynamic response of this sensor is recorded using optical spectrum analyzer (OSA) and the data is processed using MATLAB. Spectrum is closely monitored to evaluate the accurate change in the refractive index of Ionic liquid. Experimental results clearly proved the change in refractive index of Ionic liquid due to absorption of CO_2.

ACKNOWLEDGMENTS

I would like to express my deepest gratitude towards my adviser Dr. Hai Xiao, for his never ending support all the time. I am so grateful to him for providing me financial support and invaluable teaching. Dr. Xiao always has been a great source of motivation while guiding me through important aspects of my graduate career. I am also thankful to Dr. Fan Shi from Department of Energy (DOE) for providing me his valuable suggestions in this project.

I would like to extend my thanks to Dr. Mehdi Ferdowsi and Dr. Maciej Zawodniok for serving as my thesis committee. I am so grateful to Photonics Lab group for their continuous support and guidance throughout my thesis.

Finally, I would like to dedicate my thesis to my father Mr. Abdul Sattar; my mother Mrs. Razia Begum, my brother Mr. Mohammed Wajeed and rest of my family whose constant love and support encouraged me to pursue my Master's degree in USA. This project was supported by Department of Energy (DOE).

TABLE OF CONTENTS

Page

LIST OF ILLUSTRATIONS

Page

ACRONYMS

Symbol	Description
GHF	Green House Gases
FPI	Fabry-Perot Interferometer
EFPI	Extrinsic Fabry-Perot Interferometer
SMF	Single mode fiber
OSA	Optical Spectrum Analyzer
fs	Femtosecond laser
CO_2	Carbon-di-oxide

1. INTRODUCTION

1.1.MOTIVATION OF CO_2 SENSING/MONITORING

Due to a rapid increase in anthropogenic pollutants, GHG (Greenhouse gas) sensing has become one of the most researched topics in recent years. Along with the other GHGs, CO_2 is also seen consistently aggregating in the atmosphere as shown in the Figure1.1 below.

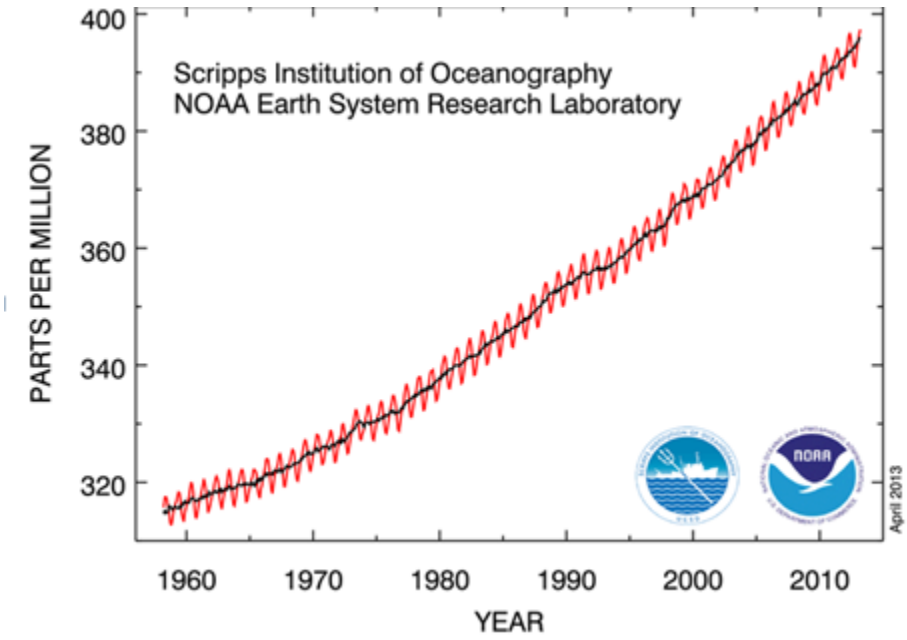

FIGURE 1.1. CO_2 CONCENTRATION IN ATMOSPHERE, MEASURED AT MAUNA, LOA, HAWAII**[1]**

The reason behind special interest on CO_2 among GHGs is that the CO_2 is rapidly growing in atmosphere due to an increase in burning of fossil fuels. Atmospheric concentration of CO_2 has been increased by more than 30% since pre-industrial stage and

till continues to increase [1]. For the US, energy related CO_2 emissions accounted for more than 99% in 2011 with electricity generation accounting for 40% of the total [2].

1.2.LITERATURE REVIEW

Optical fiber sensors are profoundly being used now due to their distinctive advantages over conventional sensing techniques. These advantages include immunity to electromagnetic interference, survivability in chemical/corrosive environment, and high sensitivity making the optical fiber sensors ideal to measure physical (e.g., stress, temperature, pressure, refractive index, etc.) and chemical (e.g., pH, chemical concentration, humidity etc.) parameters. The dynamic range and resolution of optical sensors can potentially be much greater than conventional sensors [3, 4]. Due to their survivability in chemical environment, optical fiber based devices are widely used in chemical sensing and applications.

In past two decades, gas sensors based on the laser diode absorption spectroscopy have been transformed from research models to commercial products. High sensitivity and selectivity is achieved with sophisticated signal processing techniques. Invention of Quantum cascaded laser (QCL) sensing by Bell laboratories in 1994 provided high power sources at room temperature in MWIR (Mid wavelength Infrared) region [6]. QCL operates similar to conventional laser diodes; however, photons are produced from intersubband transitions rather than recombination processes. Uniqueness of QCL lies in their ability to re-inject the transition photon into subsequent hetero-structure (Typically Ga/As or InGaAs/AlInAs) creating a cascaded effect of Laser [5]. Rapid progress in the research related to QCL lead to its acceptance in wide range of applications in absorption

based gas sensing [6, 7]. DFB (Distributed feedback) QCLs provide emission of single wavelength with wide tuning range in MWIR [7]. However, Quantum cascaded laser's component cost and manufacturability as well as the availability of high-performance supporting optical components and detectors remains a challenge for commercial products, prototype demonstrations in automotive, environmental, biomedical, and security applications during the previous decade [8]. Among absorption spectroscopy methods, Hallow waveguide sensing has also shown promise as sensitive means of detection in gas sensing, however, its large optical length requirement in absorption based sensing denied it preference over FPI cavity based sensors [7].

Fabry Perot Interferometers are particularly attractive owing to their small cross sensitivity and extremely small form factor [9]. Fabry-Perot Interferometer (FPI) has been widely used in sensing temperature, pressure, strain, refractive index, etc. [10]. FPI sensors are classified into two major types: Intrinsic Fabry-Perot Interferometers (IFPI) and Extrinsic Fabry-Perot Interferometers. EFPI sensors are usually made using two sections of same or different type of optical fibers, fused to an external housing whereas IFPI sensors made within a single fiber. Due to fusion of different fibers, EFPIs have high coupling loss and difficulty while bonding. Most of the EFPIs are fabricated in closed cavity which restricts their application to physical parameters [11, 12]. The IFPI sensors with fiber cavity fabricated inside the fiber itself, can overcome the disadvantages of EFPI sensors. However IFPI sensors struggle with low reflectivity due to small refractive index change along the sensor cavity [13, 14, 15]. In recent times so many techniques were used to fabricate FPI sensors, like direct fabrication using Femtosecond laser by Rao et al, hybrid structured type, mechanical fusion of hollow glass tube and FPI

at the tip of SMF using electric arc fusion of silica tube. N.A.S.A. has used the FPI sensing technique to sense CO_2 and CH_4 in recent times [16]. Use of photonic crystal fiber (PCF) and Multi-mode fiber (SMF) can also be seen in past publications.

1.3.IMPORTANCE OF IONIC LIQUIDS

To capture the CO_2 emissions, techniques being used in power plants are classified in to three main types:

1. Pre-combustion type
2. Post-combustion
3. Oxy-combustion.

Most widely used technique among above three is Post-combustion, in which flue gases are scrubbed against CO_2 lean solvent to remove 85-90% of CO_2 [17]. Latest technologies for CO_2 removal are using inorganic alkali and aqueous amine solutions. However use of inorganic alkaline cause serious corrosion damage to the equipment and formation of carbonate lead to high costs and energy during the absorption solution regeneration; and use of alkanolamines also cause several concerns like corrosion of amine system, extra cost, degradation at high temperature especially during regeneration, oxidative degradation and volatility, due to which they tend to get lost in the gas stream [18].

In recent times, extensive research has been conducted to replace these conventional solvents and a novel solvent; Ionic liquid is discovered. Ionic liquids are proved to have tremendous characteristics as CO_2 lean solvent. Ionic liquids are basically molten salts possessing properties like excellent thermal and chemical stability, almost

undetectable vapor pressure, wide liquid state range of about 300ºK and non-toxicity made Ionic liquid, a unique solvent in CO_2 capturing field [18, 19]. Ionic liquids are called as Green solvents in contrast to conventional solvents due to their negligible vapor-pressure. The Ionic-liquid used for the results presented in this thesis was 1-Butyl-3-methylimidazolium bis(trifluoromethylsulfonyl)imide; abbreviated as [BMIM][TF_2N] from Sigma-Aldrich. This particular Ionic-liquid has got empirical formula of $C_{10}H_{16}F_8N_3O_4S_2$, and molecular weight as 419.36 grams/mole. The structure of [BMIM][TF_2N] is shown in Figure 1.2 below.

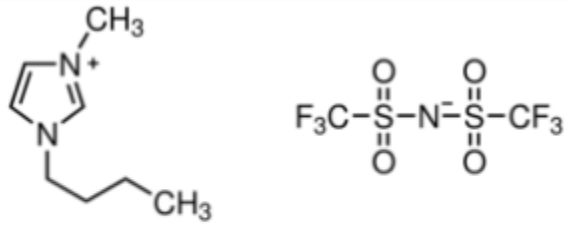

FIGURE 1.2. STRUCTURE OF [BMIM] [TF_2N]

In past, detailed research was conducted to find out the specifications of this particular Ionic liquid [20]. In a dissertation submitted to the University of Notre Dame, it was reported that the [BMIM][TF_2N] has temperature density relation as,

$$\text{Density } (gm/cm^3) = (-9.5 \text{ X } 10^{-4}) \text{ x } T(^0C) + 1.46 \qquad (1.3.1)$$

Henry constant is an important term to define the absorbing capability of any solvent. The same source has proved that Henry constant of [BMIM][TF_2N] at room temperature is

$$H\ (bar) = \quad 33.0 \pm 1.4 \qquad (1.3.2)$$

Henry constant is desired to be smallest to have higher affinity for absorption.

It was also proved that Ionic Liquid with 'TF_2N' anion has higher affinity towards CO_2 compared to many Ionic liquids with other anions. Further, it was also reported that solubility of CO_2 in [BMIM][TF_2N] is inversely proportional to temperature and directly proportional to pressure. Temperature and pressure relationship of [BMIM][TF_2N] absorbance is clearly shown in the Figure 1.3 below.

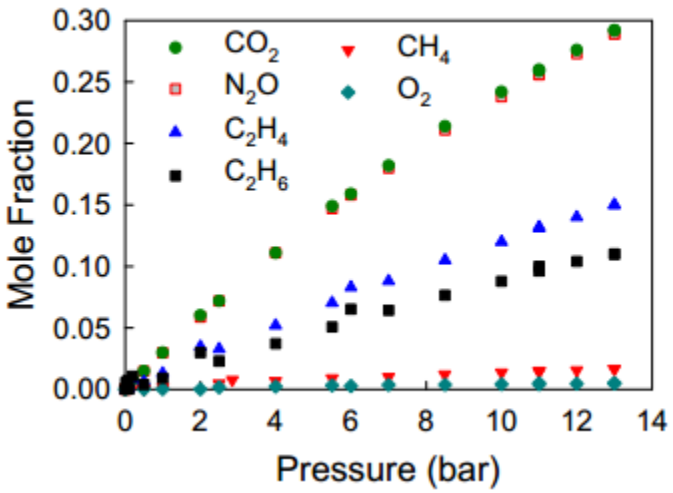

FIGURE 1.3. SOLUBILITY OF DIFFERENT TYPE OF GASES IN [BMIM][TF_2N] AT 25^0C [20]

1.4.GENERAL PRINCIPLE OF FABRY-PEROT INTERFEROMETER

The principle of Fabry-Perot was first explained by Fabry & Perot in 1899. Fabry-Perot type sensors basically use multiple mirror reflections to observe the pattern of interference. One such type of Fabry-Perot is shown below where FPI is formed with glass tube housing between two Single mode fibers. Ends of both SMF and Silica tube are properly cleaved to avoid losses.

Figure 1.4 on the next page shows a basic structure of Fabry-Perot interferometer where light of wavelength λ is incident on the parallel plates and is reflected many times by the semi-reflecting surfaces. However, light will only be transmitted across to the other side when all the multiply-reflected waves arrive together in phase – i.e. when the path difference between them is an integral number of wavelengths.

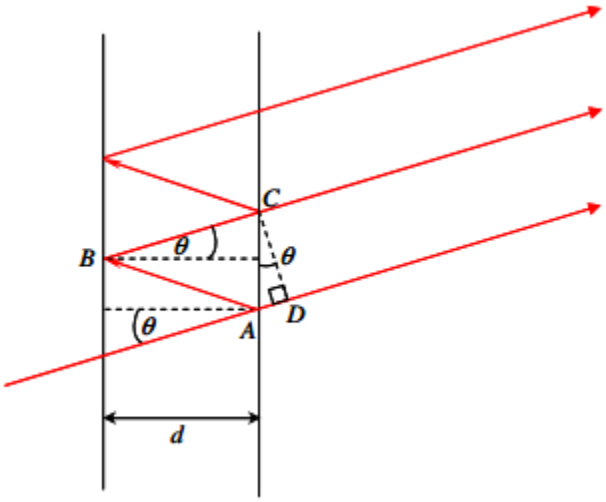

FIGURE 1.4. SCHEMATIC REPRESENTATION OF FABRY-PEROT CONFIGURATION [21]

For the two adjacently transmitted beams in Figure 1.4 above (i.e. only two-beam interference), the path difference between these is given by:

$$\text{Path Difference} = (AB + BC) - AD \qquad (1.4.1)$$

Applying simple trigonometry will yield it to be

$$= 2d \cos\theta \qquad (1.4.2)$$

(Notice that Equation (1.4.2) indicates that, for a fixed *d*, the path difference is largest when $\theta = 0^o$) Constructive interference occurs between two given beams whenever their path difference is an integral multiple of λ: i.e. $= N\lambda$, where *N* is an integer.

Thus, the condition for bright fringes (constructive interference) for the beams in Figure 1.4 is:

$$2d \cos\theta = N\lambda \qquad (1.4.3)$$

If light is arriving on the plates from many different directions (i.e. the light source is diffused rather than collimated as implied in Figure 1.4) then, a circle of bright light (i.e. subtending the same θ) will be observed, corresponding to all the possible beams that constructively interfere with a path difference of $N\lambda$. The next innermost (say) circular fringe will correspond to a smaller θ for which the path difference is $(N+1)\lambda$.

For a two-beam interferometer, such as a Michelson instrument, one can then show that the intensity *I* of the fringes varies with the phase δ (where $\delta = 2/\lambda = 4d\cos\theta/\lambda$) as :

$$I = I_0 \cos^2\left(\partial / 2\right) \qquad (1.4.4)$$

When multiple interfering beams are involved (i.e. where we consider all possible multi-reflected emerging beams at a given angle to the right in Figure 1.4, not just the bottom two), the fringes observed obey similar rules to those above but become much sharper. Then, for the Fabry-Perot multiple-beam interference, the intensity varies with δ as:

$$I_{reflection} = \frac{I_0}{1+[4R/(1-R)^2]\sin^2(\partial/2)} \qquad (1.4.5)$$

Where $I_{reflection}$ is intensity of reflections and R is the reflectivity of the interferometer plates.

Figure 1.5 shows Equation (1.4.5) plotted for different values of *R*. Notice that increasing *R* makes the fringes get much sharper (i.e. the *"resolving power"* of the instrument increases). The phase parameter δ (= $4\pi d \cos\theta/\lambda$) is essentially a measure of the angle θ, so each successive peak in Figure 1.5 represents the intensity of a circular fringe or ring at a given corresponding θ.

The quality of the metal cavity in FPI is measured in terms of finesse F. The FPI with higher finesse will give a sharper transmission peak. In Figure 1.5 the 95% reflectivity curves has the highest finesse and 4% has got the least. F is defined as following:

$$F = \frac{4R}{(1-R)^2} \qquad (1.4.6)$$

In this thesis, the finesse used is lesser than 4% because the refractive index difference between fiber and Ionic liquid is smaller than that of fiber and air.

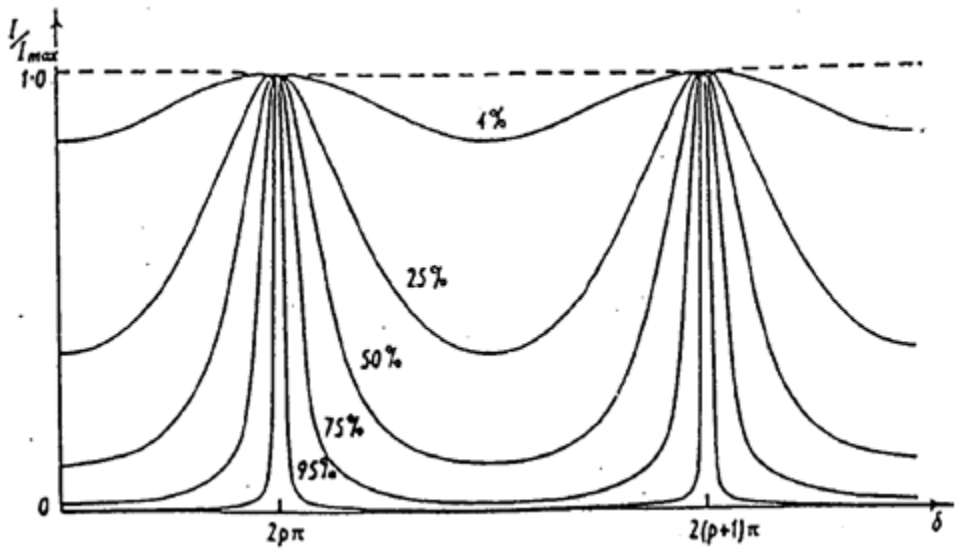

FIGURE 1.5. NORMALIZED INTENSITY IN FPI AS A FUNCTION OF THE PHASE Δ, FOR INCREASING R [21]

1.5.RESEARCH OBJECTIVE

The main objective of this thesis was to design and fabricate an open cavity based EFPI and to develop a CO_2 sensor for environmental applications. Specific objectives of the research were as following:

1. Construct an EFPI with an open cavity using Femtosecond laser.
2. Develop a CO_2 sensor employing EFPI and Ionic liquids for various applications.
3. Perform in-situ monitoring of EFPI based CO_2 sensor.
4. Prove the efficiency of Ionic liquid as CO_2 lean solvent through monitoring refractive index change.

2. SENSOR FABRICATION AND PRINCIPLE OF MEASUREMENT

2.1.FABRICATION

Desired structure is an EFPI based on a cavity fabricated using a Femtosecond laser machining. Fabrication of the sensor in this thesis is classified into two phases: in the first phase, an inline FPI is constructed using Arc fusion welding of a hallow glass tube between two standard SMFs and in the second phase, a cavity of desired dimension is etched into the already constructed Inline EFPI.

2.1.1. Fabrication; Phase-1. The expected outcome in the first phase of fabrication is an old technique reported as in-line fiber etalon [21]. A standard Corning, SMF-28 single mode fiber was used for the fabrication, and outer diameter of the hollow tube used was equal to the outer diameter of SMF-28. Wall thickness of the tube was 25 um. First, a cleaved-end section of SMF (lead-in fiber) was Arc-fused to the cleaved end of hollow silica tube. To cleave silica tube to the hollow tube, the polymer coated on the glass tube surface had to be removed. Other end of silica tube is then cleaved at the desired length carefully under the micro-scope. For cleaving at a precise distance under a microscope, microscope was attached to a moving stage with high resolution digital scale. Figure 2.1 below shows the sensor after phase-1 fabrication.

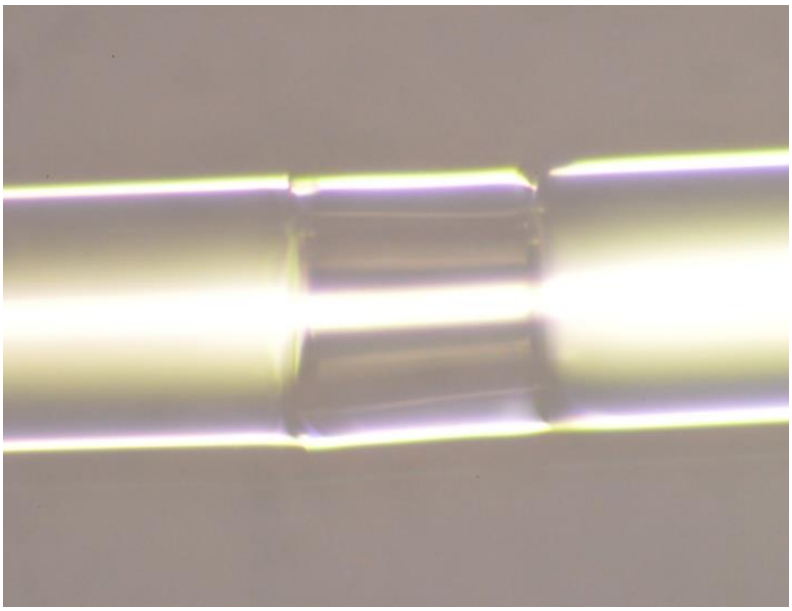

FIGURE 2.1. IN-LINE EFPI SENSOR AS SEEN THROUGH MICROSCOPE

2.1.2. Fabrication; Phase-2. This fabrication through Femtosecond laser machining is as shown in the Figure 2.2 in the next page. Femtosecond laser machining has been used several times before for creating micro-structure on silica [22, 23, 24, 25, 26]. A similar schematic diagram for fs-laser machining is shown in the Figure 2.3 in the next page. The femtosecond-laser system operates at a center wavelength of 800 nm with the repetition rate and pulse width of 250 kHz and 200 fs, respectively. The laser system provides an output of ~0.8 W which was then reduced to 40 mW by using a combination of wave plates and polarizers. An objective lens was used to focus the laser beam on the tip of the fiber to etch the cavity. The fiber was mounted on a computer-controlled five-axis translation stage (Aerotech, Inc.) with a resolution of 1 μm. So 1 μm of surface of the cavity is ablated with each scan cycle (exposure), and is exposed to the area of 70 μm × 30 μm until desired design is formed as in Figure 2.2.

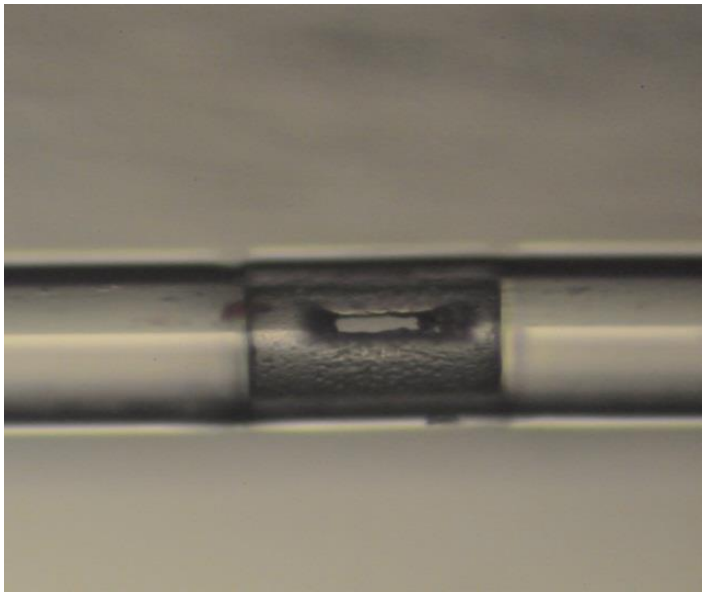

FIGURE 2.2. STRUCTURE OF CAVITY AFTER FEMTOSECOND LASER MACHINING

Fabrication process also employs a flow of inert/Nitrogen gas throughout the process of surface ablation to ensure the debris is removed away from the top surface of cavity. The cavity was cleaned using ultra-sonic wave meter before using it for the experiment.

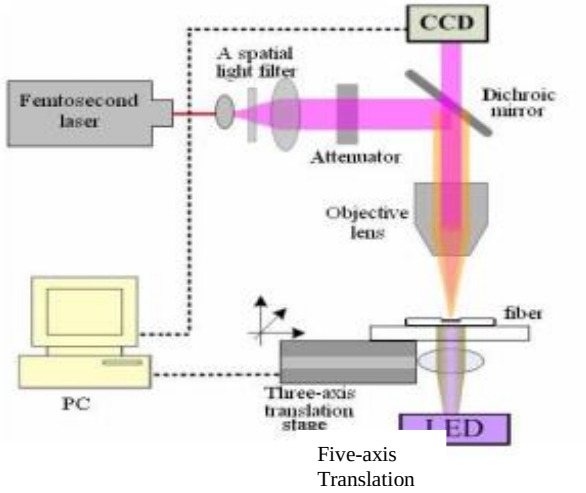

FIGURE 2.3. SCHEMATIC DIAGRAM OF FEMTOSECOND LASER MACHINING [27]

2.2.PRINCIPLE OF MEASUREMENT

2.2.1. FPI Fundamental. A typical Fabry-Perot interferometer uses arrangement of parallel surfaces kept at a specific separation with each other. Light from these surfaces get partially reflected and superposition of multiple beam of reflected light forms an interference pattern. The Figure 2.4 below shows a basic type of FPI sensors. The SMF on left hand side is a lead-in fiber fused to the other SMF on right hand side through a silica tube housing in between acting as FPI cavity. In the structure used, the fiber end of lead-out fiber was made rough to eliminate its reflection. Therefore, two mirrors are formed in the structure below; one is at the interface (interface-1) of lead-in fiber and silica tube, and the other at the interface (interface-2) of tube and lead-out SMF.

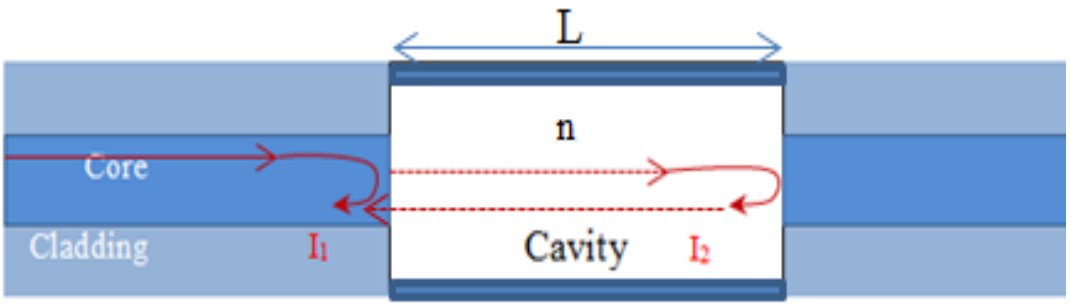

FIGURE 2.4. SCHEMATIC DIAGRAM OF FPI SENSOR

Incident light from source gets partially reflected by the first interface-1 as I_1 and partial of remaining light gets reflected at interface-2 as I_2. I_1 and I_2 superimpose with each other and generate a signal proportional to optical properties of the FPI cavity.

2.2.2. Sensing Mechanism. A typical interface of glass and air produces reflectivity of 4%. However, the cavity used in this thesis was a silica tube filled with Ionic liquid. Therefore, the interface of glass and Ionic-liquid produce reflection less than 4%. Under these conditions, FPI cavity is commonly referred to as low-finesse cavity and its waveform is explained in Figure 1.4 in the page-9. While reflectance can be numerically calculated as [29]

$$R = \left(\frac{n_{fiber} - n_{i.liquids}}{n_{fiber} + n_{i.liquids}} \right)^2 \qquad (2.2.2.1)$$

Whereas, R is reflectance,

n_{fiber} is refractive index of SMF-28; 1.4682 at 1550nm as per Corning specifications,

$n_{i.liquids}$ is refractive index of Ionic-liquids inside the cavity.

This FPI can be modeled as two beam interference model as given in equation 2.2.2.2. The equation shows that the Irradiance (power per unit area) is directly proportional to the length and refractive index of cavity.

$$I = I_1 + I_2 + 2\sqrt{I_1 I_2} \cos\left(\frac{4\pi nL}{\lambda} + \phi_0 \right) \qquad (2.2.2.2)$$

Where $I_1, I_2 =$ Intensity of reflections at surfaces,

n = refractive index, L= length of the cavity,

$\lambda =$ Wavelength of the spectrum; $\phi_0 =$ initial phase of the interference.

A sample interference spectrum of FPI is shown in the Figure 2.5 in the page-17, with adjacent valleys marked.

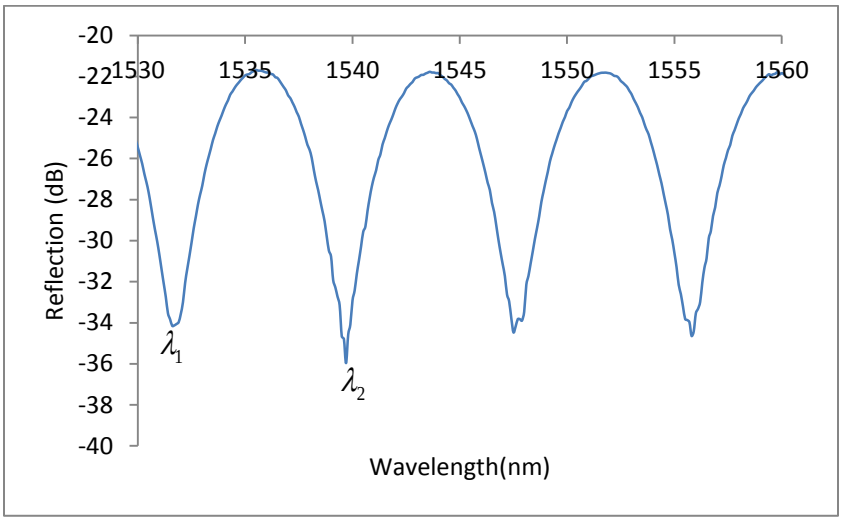

FIGURE 2.5. REFLECTION SPECTRUM OF AN FPI

The phase difference between two peaks/valley of interference should be equal to 2π, using which the refractive index change of medium can be monitored during the experiment as

$$\frac{4\pi Ln}{\lambda 1} - \frac{4\pi Ln}{\lambda 2} = 2\pi \qquad (2.2.2.3)$$

Where $\lambda 1, \lambda 2$ are two adjacent valleys/peaks of interference spectrum

L is length of the cavity,

Resolving eq 2.2.2.3 refractive index can be calculated as

$$n = \frac{\lambda 1 \lambda 2}{(2L)(\lambda 2 - \lambda 1)} \qquad (2.2.2.4)$$

Owing to its sensitivity towards optical properties of the cavity, wavelength of the FPI spectrum will shift. The deviation in wavelength is tracked to calculate the change in refractive index of Ionic-liquids as ϕ^1.

Where $$\phi^1 = \frac{4\pi L(n + \Delta n)}{(\lambda + \Delta\lambda)} \qquad (2.2.2.3)$$

The change in wavelength $\Delta\lambda$ of the interference spectrum will be proportional to the change in refractive index Δn of the Ionic-liquids that is due to the absorption of CO2 in Ionic-liquids.

3. EXPERIMENTAL METHODOLOGY

3.1.EXPERIMENTAL SET-UP

A standard single mode fiber SMF-28 sensor was connected to a 3dB coupler. As shown in the Figure 3.1 below, one end of the coupler is connected to a Broadband light source.

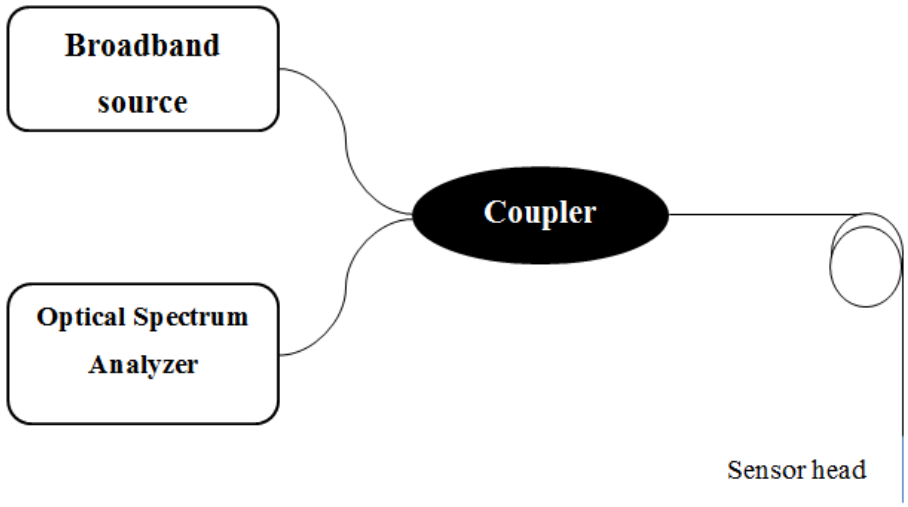

FIGURE 3.1. SCHEMATIC DIAGRAM OF SENSOR CONNECTION

Broad band sources used in this research is made by multiplexing C-band and L-band erbium-doped fiber amplified spontaneous emission (ASE) sources, which can cover the spectral range of 1530 to 1610 nm. Interference fringes reflected at sensor through coupler are recorded using an OSA (Optical Spectrum Analyzer) as shown in Figure 3.1 above.Ionic-liquid is injected in to the cavity using a long tapered glass tube, connected to a pharmaceutical syringe as shown in Figures 3.2 and 3.3.

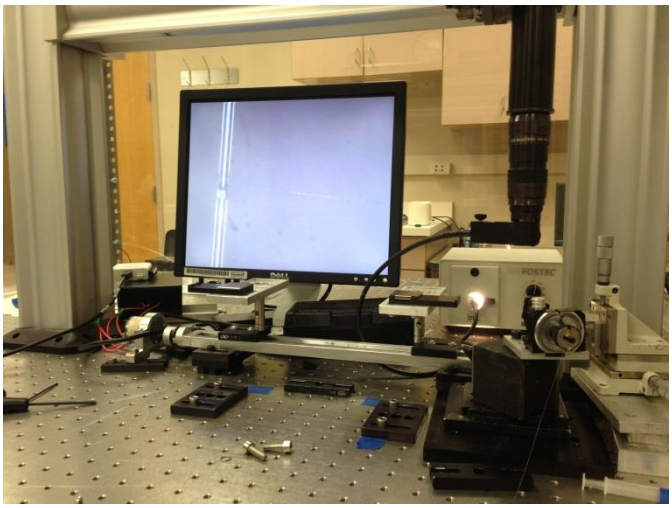

FIGURE 3.2. EXPERIMENTAL SET-UP FOR IONIC LIQUID INJECTION

Cavity and the syringe are fixed on 3-dimenstionally movable stages respectively under the microscope. Both the stages are adjusted to bring syringe in to a suitable position to inject Ionic-liquid in to the cavity. In every trial of experiment it is ensured that Ionic-liquid inside the cavity does not contain any air-bubbles to avoid ambiguity in the interference pattern. Use of ultra-sonic waves also eliminates air bubbles if there are any.

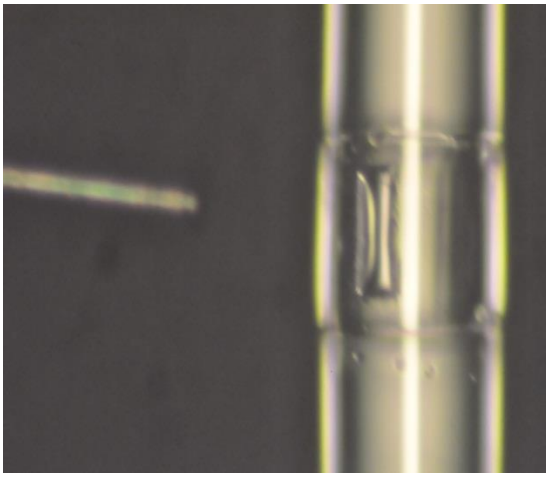

FIGURE 3.3. STRUCTURE OF CAVITY FILLED WITH IONIC LIQUID

Ionic liquids are hydrophilic substances and it is required to regenerate them before every experiment. Imidazolium type of Ionic-liquids can have a capturing rate of up to 7.4% at room temperature when exposed to dry stream of CO_2 for 3 hours. Moreover this absorption is reversible and can be achieved by heating the Ionic-liquid for several hours at temperature close to 100^0C [18]. Figure 3.4 below shows the regeneration set-up of the ionic liquid using Furnace. Ionic liquid was heated in the furnace until 100 ^{0}C and maintained at this temperature for more than 20mins. Since, quantity of the liquid in the cavity was very low so, it is assumed that the amount of time is enough for regeneration. During the heating process, a consistent flow of Argon gas was maintained to keep Ionic liquid isolated from atmospheric moisture and gases and flow of inert gas (i.e Argon) is maintained until sensor is brought down to room temperature. CO_2 absorption experiment was carried out at room temperature to avoid temperature gradient effect in FPI sensor.

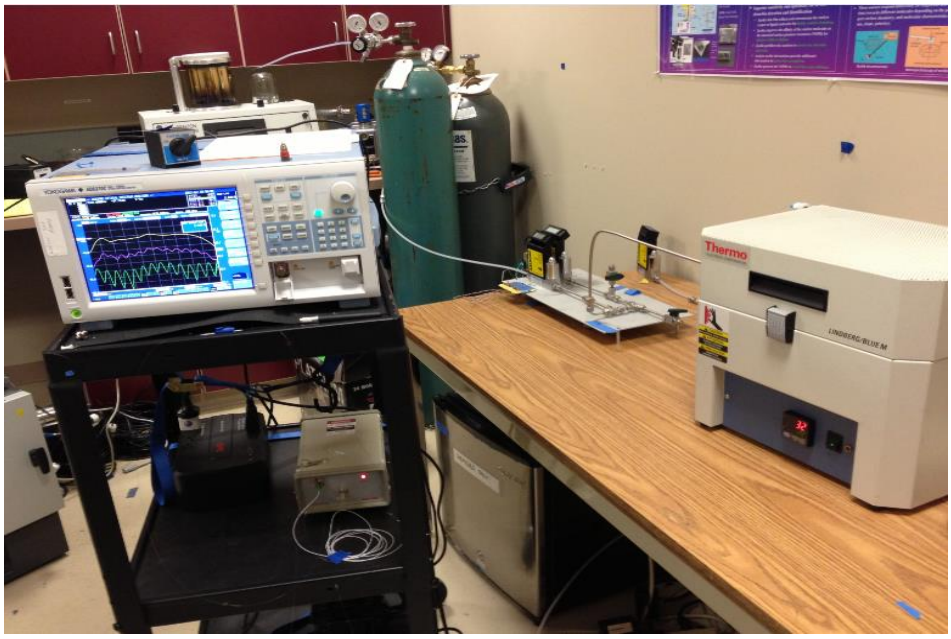

FIGURE 3.4. EXPERIMENTAL SET-UP FOR REGENERATION OF IONIC LIQUID

Flow of gas is chosen to be low, typically in range of 5-10ml/min to get rid of any fluctuation. OSA is connected to a computer with MATLAB and interference spectrums are recorded with the desired frequency. In Figure 3.5, a clear comparison is made of Ionic liquid before and after regeneration.

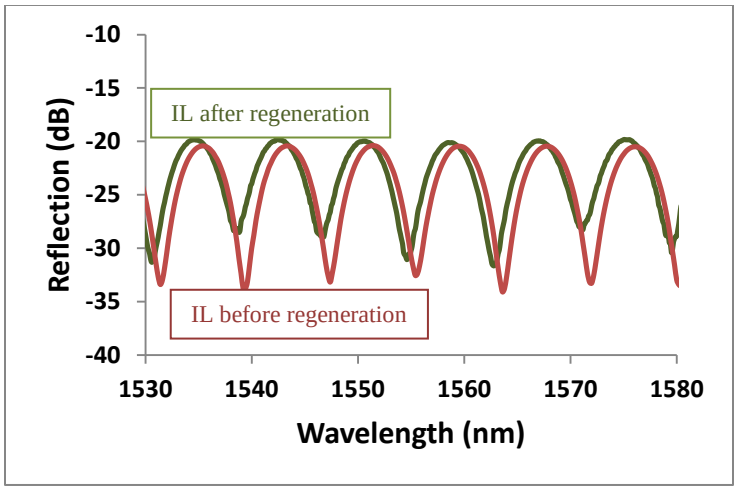

FIGURE 3.5. COMPARISON OF REFLECTION SPECTRUM

Deviation of phase and visibility is seen after regeneration in Ionic liquids after sensor was placed in the furnace and temperature is raised until 100^0C. Shift in wavelength was measured to be slightly more than 1nm towards left. Applying phase matching condition mentioned earlier in equation (2.2.2.4) refractive index deviation can be calculated as

$$n = \frac{\lambda 1 \lambda 2}{(2L)(\lambda 2 - \lambda 1)}$$

Refractive index of liquid came out as 1.469 whereas after regeneration refractive index shift to be 1.398. This shift could be due to absorption of moisture in the store room or during injection of liquid in to the sensor.

4. RESULTS AND DISCUSSION

4.1.APPLICATION

Refractive Index Measurement. Apart from Ionic liquid, some other fluids were also injected to investigate and confirm their refractive index. The Figure 4.1 below shows the difference in the reflection spectrums of Air(refractive index = 1), Acetone(refractive index = 1.359), Ethanol(refractive index = 1.35713) and Water(refractive index = 1.33). The Figure 4.1 shows that the reflection spectrum of air has a high reflection power when compared to other liquids indicating that that sensor assumed medium other than the air.

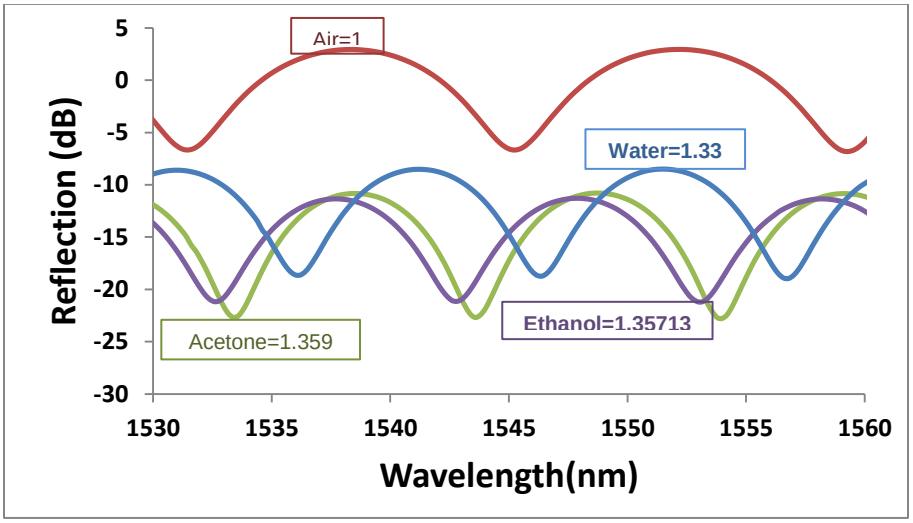

FIGURE 4.1. REFLECTION SPECTRUM OF FPI

Accurate refractive indexes were calculated using phase matching condition and the results came out to be approximately equal to the respective known refractive indices of the liquids in question.

4.2. CO2 ABSORPTION EXPERIMENT

In-situ Monitoring. As explained in section 3 of the thesis, in-situ monitoring of regeneration and absorption of CO_2 was done and the results are as shown in Figure 4.2 below.

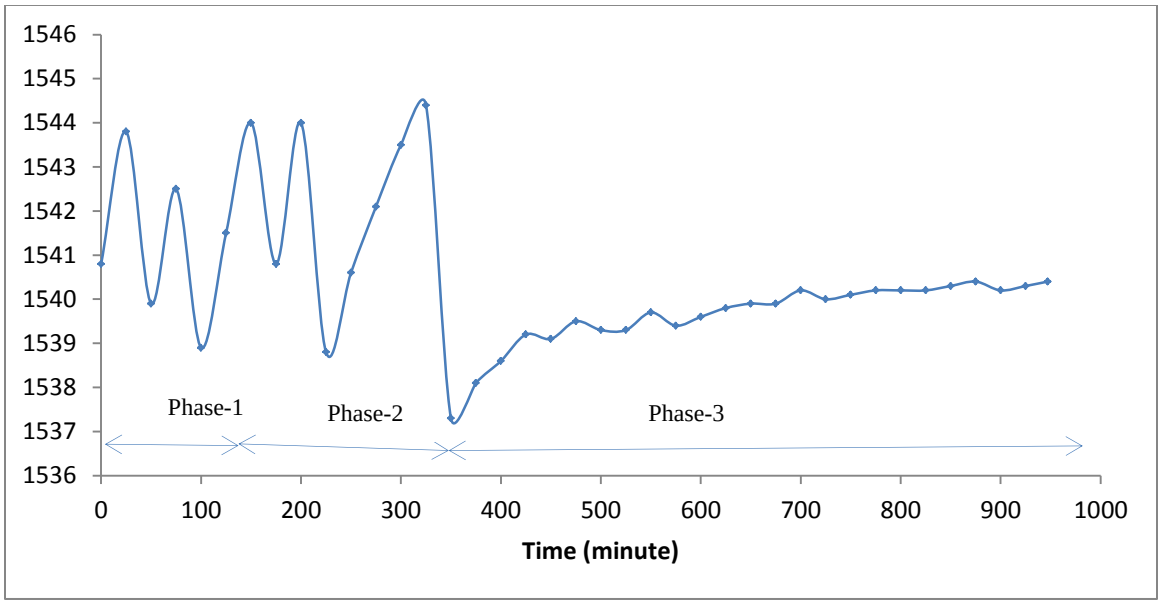

FIGURE 4.2. PHASE VS TIME GRAPH OF SENSOR

Where Phase-1 is the time period for which the sensor was heated until 100^0C in multiple steps,

Phase-2 is the time phase when the liquid was brought down to room temperature and

Phase-3 is the time when flow of CO_2 is maintained through the sensor.

A huge deviation in the phase (wavelength) is observed during phase 1 and phase 2. This might have been due to bubbling of liquid inside the sensor during positive and negative temperature gradient. Inert gas (Argon) flow of 5ml/min was maintained during phase-1and 2 to avoid any absorption of any other gas or moisture from the atmosphere.

An equal flow of CO_2 was maintained in phase-3 of the experiment as shown in Figure 4.3. Phase-3 recorded close to 2 nm of shift in first 75mins of the absorption phase and remaining 1nm shift was seen in later stage of 5 hours followed by the constant wavelength response of the sensor. As the flow of CO_2 carried out in closed and isolated (from atmosphere) chamber of furnace, shift in wavelength must be due to absorption of CO_2 by Ionic-liquids. A clear picture of phase-3 can be shown in the Figure 4.3 below where reflection spectrum is seen as consistently shifting towards right due to change in the refractive index of ionic liquid as absorption of CO_2 increases.

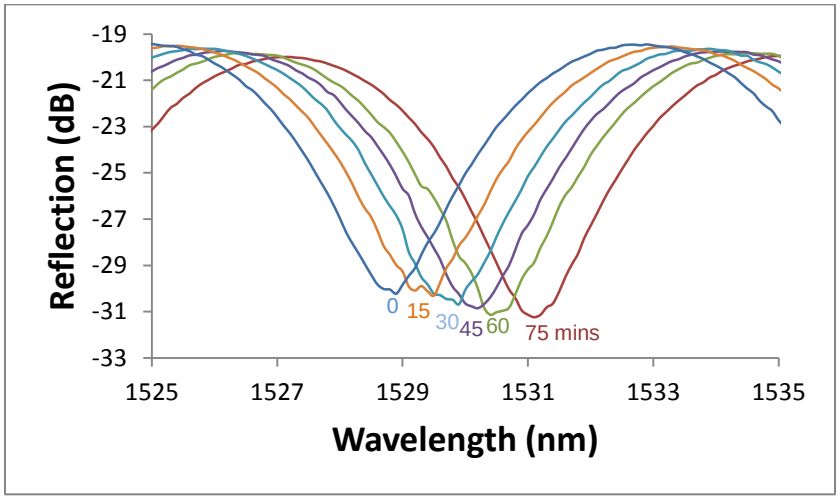

FIGURE 4.3. DEVIATION OF WAVELENGTH OF REFLECTION SPECTRUM DURING PHASE-3

In the Figure 4.3, each curve is recorded after the time intervals of 1000 Sec (16.66mins) in the beginning stage of phase-3. With each time interval, wavelength spectrum was seen shifting towards right as a enforcing our theory of absorption of CO_2 by ionic liquids. Each time interval witnessed the shift of 0.33 nm wavelength during the first 75mins of CO_2 absorption stage.

5. CONCLUSION

FPI sensors are used in wide range of applications owing to their reliability and prominence in aspects like immunity of electromagnetic interference, survivability in harsh environment, compactness etc. Recently, the EFPIs fabricated using femtosecond laser machining have attracted significant attention due to their precedence over conventional, closed cavity EFPI sensors. The limitation of inline closed cavity EFPIs have been overcome by using femtosecond micro machining with the added advantages of low power loss and better sensing properties. Ionic liquids also emerged as highly researched CO_2 absorbents in recent times due to their undeniable advantages over conventional amines. Therefore the requirement presents an opportunity for the use of EFPI for in-situ monitoring of CO_2 absorption in ionic liquids.

The thesis work is dedicated to fabricate an EFPI sensor through femtosecond fabrication, for in-situ monitoring of CO_2 absorption by ionic liquids. Experiments were conducted to find out the extent of absorption, and its effect on characteristics of EFPI. Experiments conducted successfully demonstrated the application of refractive index evaluation, for unknown fluids. The refractive indexes of Air, acetone, ethanol and water were calculated through phase matching condition of EFPI. Results obtained shown agreement with the Ideal values of fluids. $\mathbf{CO_2}$ absorption experiment was an effort through this thesis to prove the efficiency of ionic liquid as better $\mathbf{CO_2}$ lean solvent and uniqueness of the EFPI. In-situ monitoring of the experiment has witnessed a 4 nm shift in wavelength that proves absorption of $\mathbf{CO_2}$ with reference to the change in refractive index of ionic liquid.

BIBLIOGRAPHY

[1] Dr. P. Tans and Dr. Keeling, "Full Mauna Loa CO2 record," ESRL, Hawaii, 2013.

[2] H. Bovensmann, M. Buchwitz, J. P. Burrows, M. Reuter, T. Krings, K. Gerilowski, O. Schneising, J. Heymann, A. Tretner, and J. Erzinger "A remote sensing technique for global monitoring of power plant CO2 emissions from space and related applications,".

[3] " Electric Power Annual," Energy Information Administration, 2011.

[4] Jose Miguel Lopez-Higuera, "Optical sensors," University of Cantabria.

[5] E. Udd, Fiber Optic Sensors; An Introduction for Scientists and Engineers. New York: John Wiley and Sons, 1991.

[6] Faist. J, Capasso. F, Sirtori. C, Sivco. D. L, Hutchinson. A. L, Cho. A. Y. Science 1994, 264, 553-558

[7] A. Kosterev and F. Tittel, "Chemical sensors based on quantum cascade lasers," *IEEE,* vol. J. Quantum Electron, no. 38, pp. 582-591, 2002.

[8] C. Charlton, F. de Melas, A. Inberg, N. Croitoru and B. Mizaikof, "Hollow-waveguide gas sensing with room-temperature quantum cascade lasers," *IEEE,* vol. Proc. Optoelectron, no. 150, pp. 306-309, 2003.

[9] M. G. Allen, "Challenges and Opportunities for Next Generation Diode Laser Active Sensing," *IEEE,* vol. Physical Sciences Inc.

[10] Hae Young Choi, Kwan Seob Park, Seong Jun Park, Un-Chul Paek,Byeong Ha Lee and Eun Seo Choi, "Miniature fiber-optic high temperature sensor based on a hybrid structured Fabry–Perot interferometer".

[11] Y. J. Rao, "Recent progress in fiber-optic extrinsic Fabry-Perot interferometric sensors," vol. Opt. Fiber Technol, no. 12, pp. 227-237, 2006.

[12] Vikram Bhatia, Kent A Murphyz, Richard O Clausy, Mark E Jonesz, Jennifer L Gracez, Tuan A Tranz and Jonathan A Greene, "Optical fiber based absolute extrinsic Fabry - Perot interferometric sensing system," Vol. 7, Meas. Sci. Technol. pp. 58-61 , 1996.

[13] Jiangdong Deng, Pickrell.G, May R.G , Anbo Wang, and H. Xiao, "Single-crystal sapphire fiber-based strain sensor for high-temperature applications," *Optic Info Base,* vol. 21, J. Lightwave Technol., pp. 2276-2283, 2003.

[14] Y. Zhang, X. Chen, Y. Wang, K.L. Cooper, and A. Wang, "Microgap multicavity Fabry-Perot biosensor," J. Lightwave Tech., vol. 25, pp. 1797-1804, 2007.

[15] Woo-Hu Tsai and Chun-Jung Lin, "A novel structure for the intrinsic Fabry-Perot fiber-optic temperature sensor," Phys. Soc., vol. 19, p. 682 , 2001.

[16] Z. Y. Huang, Y. Z. Zhu, X. P. Chen, and A. B. Wang, "Intrinsic Fabry-Pe´rot fiber sensor for temperature and strain measurements," IEEE Photon. Technol. Lett. 17, 2403, 2005.

[17] "Robust IR Remote sensing technique of the total column of trace gases including carbon dioxide and methane, Georgieva, E.M. Geoscience and Remote Sensing Symposium (IGARSS)," *IEEE International*, 2011.

[18] J. Davison, "Performance and costs of power plants with capture and storage of CO2," Orchard Business Centre, Stoke Orchard, Cheltenham, GL52 7RZ, UK.

[19] Jun Zhang, Guang-Fei QU, Ping NING, Yu-Huan Liu, Yu-Kun Shi, and Hui Feng, "Research progress in absorption of CO2 using task-specific ionic liquids," in *Bioinformatics and Biomedical Engineering, (iCBBE) 5th International Conference*, 2011.

[20] Cheng-Hsiu Yu, Chih-Hung Huang, and Chung-Sung Tan "A Review of CO2 Capture by Absorption and Adsorption," *Taiwan Association for Aerosol Research.*

[21] J. L. Anthony., "Gas Solubilities in Ionic Liquids: Experimental measurement and applications; A dissertation of Phd," University of Notre Dame.

[22] Department of Physics., University of Surrey, "FABRY-PEROT INTERFEROMETER," General physics experiment.

[23] J. S. Sirkis, D. D. Brennan, M. A. Putman, T. A. Berkoff, A. D. Kersey, and E. J. Friebele "In-line fiber etalon for strain measurment," *OSA*, vol. 18, no. Optics Letters, p. 22, 1993.

[24] A. Marcinkevi Ius, S. Juodkazis, M. Watanabe, M. Miwa, S. Matsuo, H. Misawa, and J. Nishii, "Femtosecond laser-assisted three-dimentional microfabrication in silica," *OSA*, vol. 26, no. Opt. Lett. , pp. 277-279, 2001.

[25] Y. Lai, K. Zhou, L. Zhang, and I. Bennion "Microchannels in conventional single-mode fibers," *OSA*, vol. 31, no. Opt. Lett. , pp. 2559-2561, 2006.

[26] Adriaan van Brakel, Christos Grivas, Marco N. Petrovich, and David J. Richardson, "Microchannels in conventional single-mode fibers," *31, 2559-2561(2006)*, vol. 15, no. Opt Express, pp. 8731-8736, 2007.

[27] D. Lorenc , D. Velic, A.N. Markevitch, R.J. Levis "Adaptive femtosecond pulse shaping to control supercontinum generation in a microstructure fiber," no. Opt. Commun, pp. 276, 288-292, 2007.

[28] Francis Hindle, Eric Fertein, Christophe Przygodzki, Florian Dürr, Laurent Paccou, Robin Bocquet, Pierre Niay, Hans Georg Limberger, and Marc Douay "Inscription of long-period gratings in pure silica and germano–silicate fiber cores by femtosecond laser irradiation," *IEEE Photon.*, vol. 16, no. Technol. Lett., pp. 1861-1863, 2004.

[29] Yun-Jiang Rao, Ming Deng, De-Wen Duan, Xiao-Chen Yang, Tao Zhu, Guang-Hua Cheng, "Micro Fabry-Perot interferometer in silica fibers machined by femtosecond laser," *OSA*, vol. 15, no. Optics Express, pp. 14123-14128, 2007.

[30] E.Hecht, Optics, Addison Wesley, 2002.

[31] Comittee members, "Front Matter." Verifying Greenhouse Gas Emissions: Methods to Support International Climate Agreements., Washington, DC: The National Academies Press, 2010.

VITA

Mujahid Abdul was born in Tandur, Andhra Pradesh, India. He obtained his B.E. degree in Instrumentation Engineering from Deccan College of Engineering & Technology affiliated to Osmania University in August 2009. In December 2009 he started working as GIS Representative at Google maps (though SERCO), and resigned as an Assistant team in August 2011. He joined graduate program in Electrical Engineering in August 2011 at Missouri S&T. He received his Master of Science degree in Electrical Engineering from Missouri S&T in August 2013. His research interest includes Optical sensors and Instrumentation.